

Analysis and design of power and bandwidth of nonlinear vibration energy harvesters with hardening restoring forces*

Arata Masuda*

Faculty of Mechanical Engineering, Kyoto Institute of Technology, Matsugasaki Goshō-Kaidō-Cho, Sakyo-Ku, Kyoto 6068585, Japan

Abstract

This paper presents a theoretical foundation for designing the power and bandwidth performance of an electromagnetic nonlinear vibration energy harvester with a hardening resonator. To this end, the steady-state solution derived via first-order approximation is investigated to establish a graphical approach, which gives a clear perspective on how the resonance peak point on the frequency-displacement curve is determined in terms of the excitation amplitude, nonlinear restoring force function, and other design parameters. Then, a ν -power bandwidth, a generalized version of the half-power bandwidth, is newly introduced and its approximate analytical formulation is derived. Based on the findings of the parameter study on the ν -power bandwidth, a design scheme is proposed, which begins with specifying the location of the resonance peak point that guarantees the existence of the high-energy branch under possible variations of the excitation, followed by determining the linear natural frequency that makes the ν -power bandwidth as large as reasonably possible. Design examples, assuming a specific class of hardening nonlinearity of the restoring force, are shown to demonstrate how the proposed design scheme yields vibration energy harvesters with maximized power bandwidth performance while incorporating given design requirements.

Keywords: vibration energy harvesting, nonlinear, hardening, design, power, bandwidth

1. Introduction

A vibration energy harvester utilizes a mechanical resonator furnished with an electromechanical transducer to efficiently capture the mechanical energy from an environment vibration source and convert it to electric energy. In earlier works, single-degree-of-freedom linear resonators were preferred because of their mechanical simplicity. In the linear design, the natural frequency of the resonator has to be matched with the dominant frequency of the vibration source, and the mechanical Q factor is designed as large as possible in order to maximize the harvested power. The large Q factor, however, restricts the resonance to a narrow frequency band; therefore, the converted power decreases significantly if the dominant frequency of the source moves out of this band [1, 2, 3]. This trade-off has been well-recognized as the most critical obstacle to practical application because it requires strict tuning of the resonator to the target source, making it difficult to use under variable source conditions and hindering the deployment of harvesting devices as standard products.

The idea of introducing nonlinear resonators as a means for mitigating the power-bandwidth trade-off has attracted attention for over a decade [4, 5, 6, 7, 8, 9]. Most of the reported studies utilize Duffing-type monostable oscillators [10, 11, 12, 13, 14], zero-stiffness (essentially nonlinear) oscillators [14, 15, 16], or bistable oscillators [17, 18, 19, 20, 21]. These studies are aimed at developing a single-degree-of-freedom energy harvester that can respond largely in a wide frequency range by exploiting the dynamic behavior of nonlinear oscillators. Among them, a Duffing-type monostable nonlinear oscillator is one of the most promising methods when the vibration source has a single

*This is an Accepted Manuscript for *Journal of Sound and Vibration*, <https://doi.org/10.1016/j.jsv.2023.117575>. This manuscript version is made available under the CC-BY-NC-ND 4.0 license <http://creativecommons.org/licenses/by-nc-nd/4.0>

*Tel.: +81 75 7247381; fax: +81 75 7247300

Email address: masuda@kit.ac.jp (Arata Masuda)

dominant frequency. It can achieve a broad operation frequency range by folding the resonance peak toward the higher (lower) frequency direction by using a hardening (softening) spring instead of a linear spring. For the realization of hardening resonators, the nonlinearity due to membrane stress caused by the stretching of the neutral axis of beam resonators [22, 23] is often used. Using mechanical stoppers is another common strategy [10, 24, 25] to implement a bi-linear hardening effect in the resonator design. For softening resonators, utilizing post-buckling deformation [26] and magnetic force [12] are common ways of achieving such a realization.

Despite there being several specific designs of nonlinear harvesters in the literature, only a few works that explicitly formulate the expected power and bandwidth and provide design formulae for power-bandwidth optimization have been reported. In [27], Ramlan et al. derived a closed-form representation of the half-power bandwidth of a harvester with cubic nonlinearity based on a straightforward application of the definition of the half-power bandwidth of linear harvesters that takes the cross-section of the frequency-displacement curve with respect to the $1/\sqrt{2}$ of the peak value. Sebald et al. [28] studied the power and the bandwidth of piezoelectric energy harvesters with cubic nonlinearity. They evaluated a half-power bandwidth by directly taking a cross-section of the power-frequency curve with respect to the half of the peak value, and normalizing it by taking a ratio with respect to the peak frequency. Cammarano et al. [29] derived an analytical relationship between the power, excitation frequency, and resistive load and presented its simplification, based on which they performed optimization of the resistive load and the linear stiffness to deliver maximum power at a specific excitation frequency. In [30], Cammarano et al. presented a comparison between linear and nonlinear harvesters in terms of the half-power bandwidth numerically calculated based on the formulation derived in [29]. They also proposed a conservative definition of the bandwidth to address concerns about the uncertain operation in a frequency range where multiple stable solutions coexist.

The work presented in this paper is devoted to providing a clear theoretical perspective on the power and bandwidth design of a nonlinear electromagnetic vibration energy harvester. To achieve this goal, the steady-state solution of the equation of motion of a nonlinear harvester with a hardening resonator subject to a sinusoidal base excitation derived via a first-order approximation is adopted as the theoretical foundation. A graphical approach is proposed in Section 2.3 to visualize how the resonance peak point on the frequency-displacement curve is determined in terms of the equivalent stiffness of the nonlinear restoring force, mechanical and electrical damping, and excitation amplitude. For the definition of the bandwidth of the hardening resonator, the problem of coexisting multiple solutions is not of concern in this study, in contrast to the discussion in [30], by assuming the use of certain methodologies that guarantee operation in the highest-energy solution by injecting a part of the harvested energy into the resonator [28, 31, 32, 33, 34, 35, 36, 37, 38, 39]. Then, a generalized version of the half-power bandwidth, called ν -power bandwidth, is defined in Section 3.2, and its approximate analytical formulation is derived. The influence of the electromechanical coupling factor and load resistance on the power-bandwidth performance is discussed in Section 3.3 to elaborate on these dependencies and simplify the problem statement for building a design scheme. In Section 4, a design scheme that starts with specifying the appropriate location of the resonance point, referred to as critical resonance point (CRP), by considering possible variations of excitation frequency and amplitude, is proposed. Throughout the work, a specific class of hardening nonlinearity of the restoring force, referred to as odd-power nonlinearity, is assumed when providing calculation examples. Finally, the conclusions are summarized in Section 5.

2. Formulation

2.1. Modeling

The nonlinear vibration energy harvester investigated in this paper is modeled as a single-degree-of-freedom mechanical resonator subjected to a sinusoidal base excitation, schematically drawn in Fig. 1. The mass of the resonator is suspended by a nonlinear hardening spring with a mechanical damping element and an electromagnetic transducer installed in parallel between the mass and base. The electrical port of the transducer is connected to a load circuit, which is simplified by an equivalent pure resistance R , serially connected to the internal impedance of the transducer Z_T .

The equation of motion of the harvester is given by

$$m\ddot{x}(t) + c_m\dot{x}(t) + \Phi i(t) + f(x(t)) = -mu_a \cos \omega t \quad (1)$$

where t is the time, x is the relative displacement of the mass to the base, and i is the current flowing through the induction coil; furthermore, m , c_m , Φ , $f(x)$, u_a , and ω are the inertial mass, mechanical damping coefficient, force

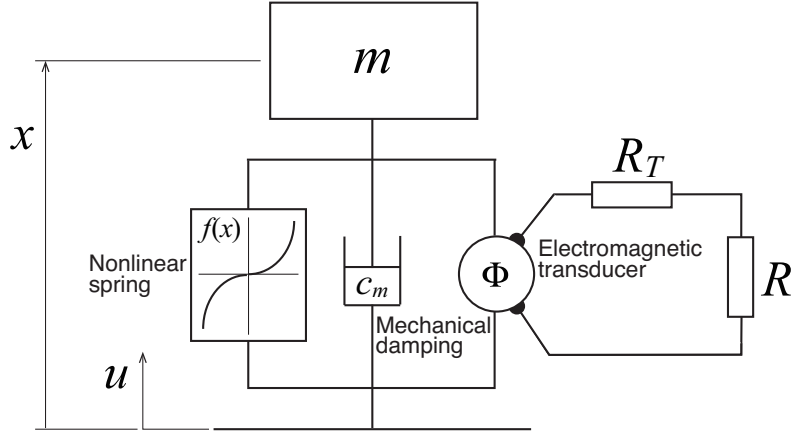


Figure 1: Model of a nonlinear vibration energy harvester. The harvester is modeled as a single-degree-of-freedom mechanical resonator subjected to a sinusoidal base excitation. The mass of the resonator is suspended by a nonlinear hardening spring with a mechanical damping element and an electromagnetic transducer installed in parallel between the mass and base. The electrical port of the transducer is connected to a load circuit, which is simplified by an equivalent pure resistance serially connected to the internal impedance of the transducer.

factor of the electromagnetic transducer, restoring force of the nonlinear spring, amplitude of the base acceleration, and excitation frequency, respectively. The nonlinear restoring force is assumed to be an odd-symmetric hardening function of the displacement with the only stable zero at the origin, i.e., $f(-x) = -f(x)$, $f'(0) > 0$, and $f'(\alpha) \leq f'(\beta)$ for any $0 \leq \alpha < \beta$, where $\{\cdot\}'$ denotes the first derivative. It should be noted that, although the damping coefficient and the force factor may also be nonlinear with respect to the displacement and velocity in a practical situation, they are assumed constant in this study for mathematical simplicity. This point will be further discussed in a later section. The formulation that considers the nonlinearity of the damping force and the force factor can be found in [32].

The electric circuit equation is given by

$$L_T \dot{i}(t) + (R + R_T)i(t) = \Phi \dot{x}(t) \quad (2)$$

where L_T and R_T are the inductance and resistance of the induction coil, respectively.

Assuming that the contribution of the inductance term in Eq. (2) is negligibly small at the excitation frequency, and eliminating the current from Eqs. (1) and (2), the governing equations are reduced to

$$m\ddot{x}(t) + c_m \dot{x}(t) + \frac{\Phi^2}{R + R_T} \dot{x}(t) + f(x(t)) = -mu_a \cos \omega t \quad (3)$$

The third term on the left-hand side of Eq. (3) is the electric damping term representing the force reacting to the velocity via electromagnetic coupling. Rewriting Eq. (3) into state equations leads to

$$\dot{x}(t) = y(t) \quad (4)$$

$$\dot{y}(t) = -\frac{1}{m} \left[\left(c_m + \frac{\Phi^2}{R + R_T} \right) y(t) + f(x(t)) \right] - u_a \cos \omega t \quad (5)$$

2.2. Steady-state solution

The steady-state solution of Eqs. (4) and (5) are derived by following the Krylov-Bogoliubov averaging method [40], by assuming the solution as $x(t) = a \cos(\omega t - \psi)$, and $y(t) = -a\omega \sin(\omega t - \psi)$, where a and ψ are the time-dependent

amplitude and time-dependent phase delay to the base acceleration, respectively. Substituting them into the state Eqs. (4) and (5) leads to a system of differential equations for the amplitude and phase delay, as follows:

$$\dot{a} = -h(a, \psi, \theta)a\omega \sin \theta \quad (6)$$

$$a\dot{\psi} = h(a, \psi, \theta)a\omega \cos \theta \quad (7)$$

where $\theta = \omega t - \psi$, and the dimensionless function $h(a, \psi, \theta)$ is defined as

$$h(a, \psi, \theta) = -\frac{-ma\omega^2 \cos \theta + f(a \cos \theta)}{ma\omega^2} + \left(c_m + \frac{\Phi^2}{R + R_T} \right) \frac{a\omega \sin \theta}{ma\omega^2} - \frac{mu_a \cos(\theta + \psi)}{ma\omega^2} \quad (8)$$

The right-hand side of Eq. (8) indicates that $h(a, \psi, \theta)$ is a 2π -periodic function of θ ; furthermore, $h(a, \psi, \theta) = O(\varepsilon)$, where ε is a positive small number ($0 < \varepsilon \ll 1$), when assuming weak damping and resonant operating conditions (see Appendix A). Thus, the left-hand sides of Eqs. (6) and (7) are again 2π -periodic with respect to θ and $O(\varepsilon)$. Therefore, Eqs. (6) and (7) are approximated by the following autonomous system, which is derived by eliminating θ by means of an averaging technique [41]:

$$\dot{a} = -\frac{c_t}{2m}a - \frac{1}{2\omega}u_a \sin \psi \quad (9)$$

$$a\dot{\psi} = -\frac{a}{2m\omega} \left(-m\omega^2 + K_{\text{eq}}(a) \right) - \frac{1}{2\omega}u_a \cos \psi \quad (10)$$

where c_t is the total damping coefficient defined as

$$c_t = c_m + \frac{\Phi^2}{R + R_T} \quad (11)$$

and K_{eq} is the equivalent stiffness defined as

$$K_{\text{eq}}(a) = \frac{1}{\pi a} \int_0^{2\pi} f(a \cos \theta) \cos \theta d\theta \quad (12)$$

The autonomous system represented by Eqs. (9) and (10) governs the slow modulation dynamics of the amplitude and phase delay of the harvester's response.

The steady-state amplitude and phase delay are derived as the equilibrium of this autonomous system. This is done by setting the left-hand sides of Eqs. (9) and (10) equal to zero, leading to

$$a^2 \left[(-m\omega^2 + K_{\text{eq}}(a))^2 + (c_t\omega)^2 \right] = (mu_a)^2 \quad (13)$$

which implicitly defines the frequency response curve for the displacement amplitude. Also, the equilibrium of Eqs. (9) and (10) gives the frequency response curve for the phase delay as

$$\psi = \text{atan2} \left(-c_t\omega, -(-m\omega^2 + K_{\text{eq}}(a)) \right) \quad (14)$$

The stability of the steady-state solution is determined by examining the Jacobian of Eqs. (9) and (10) at the equilibrium, which reduces to the stability condition given by

$$\frac{d\omega}{da} (-m\omega^2 + K_{\text{eq}}(a)) > 0 \quad (15)$$

In general, the implicit representation of the frequency response curve (given by Eq. (13) in the presented case) must be solved numerically by finding ω - a curves that equate the left-hand side and right-hand side of the equation. It can be analytically solved, however, in the presented case because Eq. (13) is a quadratic equation with respect to ω^2 . Solving Eq. (13) with respect to ω^2 for a given a followed by taking the square root gives the positive solutions of ω as

$$\omega = \sqrt{\frac{K_{\text{eq}}(a)}{m} \left[1 - 2\zeta_{\text{eq}}^2(a) \pm \sqrt{\left(\frac{mu_a}{K_{\text{eq}}(a)a} \right)^2 - 4\zeta_{\text{eq}}^2(a)(1 - \zeta_{\text{eq}}^2(a))} \right]} \quad (16)$$

where $\zeta_{\text{eq}}(a)=c_t/(2\sqrt{mK_{\text{eq}}(a)})$. This reduces to

$$\omega = \sqrt{\frac{K_{\text{eq}}(a)}{m}} \left[1 \pm \frac{1}{2} \sqrt{\left(\frac{mu_a}{K_{\text{eq}}(a)a}\right)^2 - 4\zeta_{\text{eq}}^2(a)} \right] + O(\varepsilon^2) \quad (17)$$

or

$$\omega = \sqrt{\frac{K_{\text{eq}}(a)}{m}} \pm \frac{1}{2} \sqrt{\frac{m}{K_{\text{eq}}(a)} \left(\frac{u_a}{a}\right)^2 - \left(\frac{c_t}{m}\right)^2} + O(\varepsilon^2) \quad (18)$$

by considering a small damping ratio and the resonating condition, which respectively imply $\zeta_{\text{eq}}=O(\varepsilon)$ and $mu_a/(K_{\text{eq}}a)=O(\varepsilon)$. The second term on the right-hand side of Eq. (18) is $O(\varepsilon)$, which legitimizes the assumption of $\omega = \sqrt{K_{\text{eq}}(a)/m} + O(\varepsilon)$; the first term is the backbone curve that defines the amplitude-dependent equivalent natural frequency.

The accuracy of the steady-state solution given by Eq. (16) as well as the validity of the approximation performed from Eq. (16) to Eq. (18) are verified for harvesters with odd-power nonlinearity, which is mathematically defined in Appendix B, for $n=1, n=2, n=5$, and $n=25$. The verification results are presented in Fig. 2, in which the abscissa and ordinate axes are normalized by the linear natural frequency $\omega_0 = \sqrt{k_0/m}$ and static displacement $x_{st} = mu_a/k_0$, respectively. The solid red lines and dashed red lines are the stable and unstable branches, respectively, of the resonance curves given by Eq. (16) for four different values of β , which correspond to the cases where the resonance frequency ω_r equals ω_0 (linear), $1.5\omega_0$, $2\omega_0$, and $3\omega_0$, i.e., $\gamma=1, 1.5, 2$, and 3 , where $\gamma=\omega_r/\omega_0$. Whereas, the solid and dashed black lines are the resonance curves given by Eq. (17) (or Eq. (18)) with the same configuration as the red lines, ignoring the second and higher-order terms. Furthermore, the circles and triangles show the steady-state amplitudes for upward- and downward-swept frequencies, respectively, which are obtained by numerically integrating Eq. (3) with the MATLAB ode45 scheme. From the figure, it can be observed that the steady-state solutions given by Eq. (16) derived by the averaging method agree well with the direct numerical solutions for a wide range of frequencies, even for strong nonlinearity cases, and that the approximation given by Eq. (17) (or Eq. (18)) is valid close to the resonance peaks where the red and black lines almost coincide.

The amplitude at the resonance peak a_r is derived by finding a for which the inside of the inner square root of Eq. (18) vanishes, such that

$$a_r = \frac{mu_a}{c_t\omega_r} \quad (19)$$

where the frequency at the resonance peak ω_r is derived from the first term on the right-hand side of the same equation as

$$\omega_r = \sqrt{\frac{K_{\text{eq}}(a_r)}{m}} \quad (20)$$

The above Eqs. (19) and (20) define a system of equations that implicitly determines the resonance frequency and amplitude of lightly damped nonlinear resonators, the appearance of which is formally the same as that for linear resonators.

2.3. Graphical approach

From Eqs. (20) and (19), one can define curves C1 and C2 on the (ω, a) -plane, respectively defined as

$$\text{C1: } \omega = \sqrt{\frac{K_{\text{eq}}(a)}{m}} \quad (21)$$

and

$$\text{C2: } a\omega = \frac{mu_a}{c_t} \quad (22)$$

Then, the resonance peak point (ω_r, a_r) is interpreted as the intersection of these two curves. This interpretation is legitimate as one can observe in Fig. 3 that the tip of the resonance peak is located at the intersection of C1 and C2, and plays a key role in this study, providing a geometrical perspective for the design of the nonlinear wideband electromagnetic harvester.

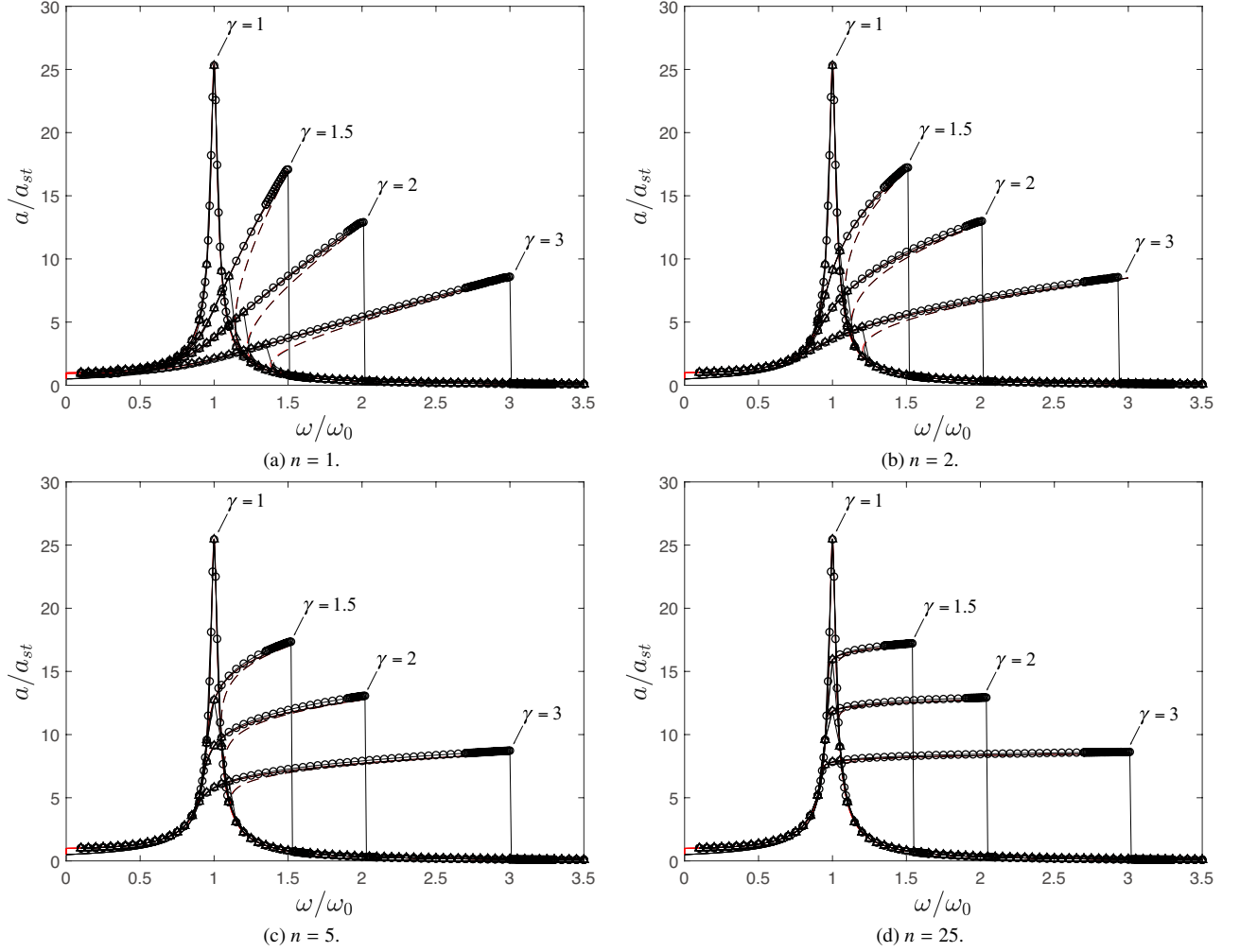


Figure 2: Verification of the frequency response curves derived by the averaging method by comparing with numerical solutions. The verification is conducted for the harvesters with odd-power nonlinearity, which is mathematically defined in Appendix B, for $n=1$, $n=2$, $n=5$, and $n=25$. The solid and dashed red lines are the stable and unstable branches of the resonance curves, respectively, given by Eq. (16) for four different values of γ , which correspond to the cases where the resonance frequency ω_r equals ω_0 (linear), $1.5\omega_0$, $2\omega_0$, and $3\omega_0$. The solid and dashed black lines are the resonance curves given by Eq. (17) (or Eq. (18)) with the same configuration as the red lines, ignoring the second and higher-order terms. The circles and triangles show the steady-state amplitudes for upward- and downward-swept frequencies, respectively, which are obtained by numerically integrating Eq. (3). (For interpretation of the references to color in this figure legend, the reader is referred to the web version of this article.)

Curve C1, drawn as a chain line in Fig. 3, is a curve called the backbone curve determined merely by the force-displacement relationship of the nonlinear spring that has a positive $d\omega/da$ everywhere due to its hardening characteristics. Whereas, curve C2 is a monotonically decreasing hyperbolic function of the frequency, shown as a bold line in Fig. 3 that depends on the mass, excitation magnitude, mechanical damping, and electrical damping quantities.

When the force-displacement relationship of the nonlinear spring is fixed, curve C1 is fixed. The larger excitation magnitude and mass, and the smaller damping (both mechanical and electrical) move curve C2 upward. Therefore, the intersection between C1 and C2, i.e., the resonance peak point, moves to a higher frequency and larger amplitude. This point of view also reveals how the load resistance R affects the resonance peak. Recalling Eq. (11), a larger load resistance makes the total damping smaller. Therefore, the resonance peak point moves rightward along backbone curve C1 as the load resistance increases, and the movement is bounded by the intersections with curves C2 for the

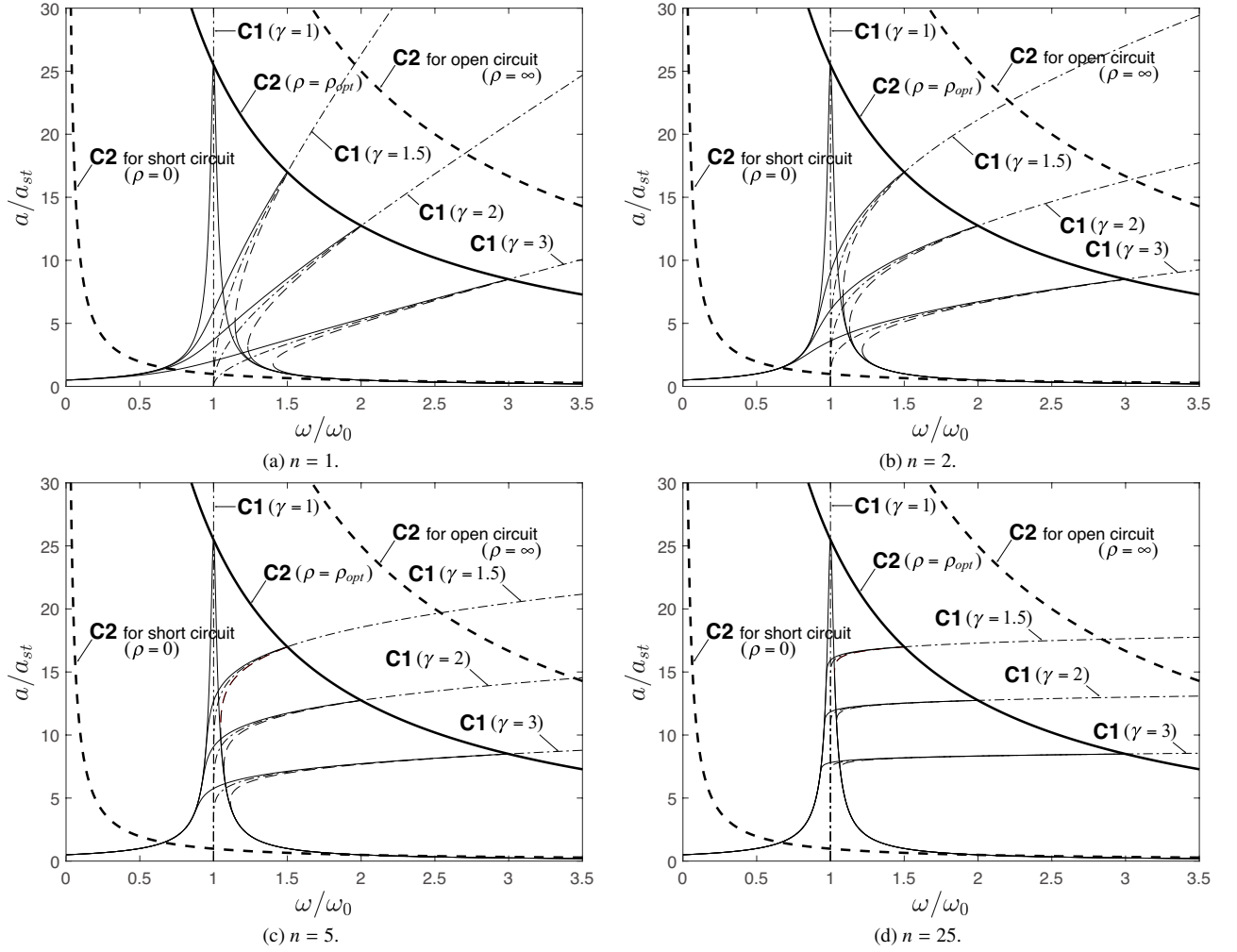


Figure 3: The resonance curves given by Eq. (17) (or Eq. (18)) for the same configuration as Fig. 2, depicted with the corresponding curves C1 and C2. This figure is shown to demonstrate how the proposed graphical approach can explain the location of the resonance peak point. Curve C2 for each case is drawn assuming optimal load ρ_{opt} , which is described in Section 3.1.

short circuit and open circuit cases that are depicted by bold dashed lines in Fig. 3.

Conversely, when curve C2 is fixed, the shape of backbone curve C1 governs where the resonance peak point will be located. Generally speaking, the more deeply bent the backbone curve is, the higher the resonance frequency. This implies that the shape of the backbone curve plays a key role in the design of the bandwidth of the nonlinear harvester, which is investigated in the next section in terms of a power-based characterization of the bandwidth.

Those rather simple tendency of the behavior of the resonance peak point relies on the monotonically increasing nature of C1 and the monotonically decreasing nature of C2, which are respectively guaranteed by the hardening nonlinearity of the spring and the linearity of the damping, both of which were initially assumed in this study. It should be emphasized that the graphical approach presented above, in which the resonance peak point is interpreted as the intersection of curves C1 and C2, is still valid even if the spring is not purely hardening or the damping is not linear. However, since one may experience more complicated situation described below in such cases, this study assumes the hardening nonlinearity and linear damping to avoid excessive complexity.

First, if the nonlinear restoring function is not purely hardening but softening or even reversible [42], backbone curve C1 is not monotonically increasing but the whole or some part of C1 has negative value of $d\omega/da$. Despite this

difference, it should be possible to conduct power-bandwidth analyses and design studies similar to those developed in this study if the intersection between C1 and C2 is single. But otherwise, one may have to consider the existence of isolated stable branches of the steady-state solution that is located between the intersections, which require more complicated and careful discussion when defining and evaluating the bandwidth of the resonance peak.

On the other hand, if the damping is nonlinear, the total damping coefficient c_t in Eq. (22) should be replaced by an equivalent total damping coefficient $C_{t,eq} = C_{m,eq} + \Phi^2/(R + R_T)$, where $C_{m,eq}$ is the equivalent mechanical damping coefficient [32]. Since the equivalent mechanical damping coefficient is generally a function of the displacement amplitude a and excitation frequency ω [43], there is no guarantee in general that C2 defined by Eq. (22) will be a hyperbola. On the contrary, it may have multiple intersections with C1 in some extreme cases, making the generalized definition of the bandwidth complicated. Nevertheless, decreasing monotonicity of C2 can be expected in many cases, (in fact, the C2 curves in the cases of velocity-squared damping [43] and Coulomb friction damping are hyperbolic because $C_{t,eq}$ is a function of $a\omega$ in both cases), where the location of the resonance peak point has the same tendency as described above, and thus the bandwidth discussion in the following sections is not affected.

For notational simplicity, an amplitude-dependent equivalent natural frequency $\omega_{eq}(a)$ is hereafter introduced as $\omega_{eq}(a) = \sqrt{K_{eq}(a)/m}$. In addition, a dimensionless load resistance ρ and dimensionless electromechanical coupling factor δ are defined as $\rho = R/R_T$ and $\delta = \Phi^2/(c_m R_T)$, respectively. Then, the equations of C1 and C2 can be rewritten as

$$\text{C1: } \quad \omega = \omega_{eq}(a) \quad (23)$$

and

$$\text{C2: } \quad a\omega = \frac{mu_a}{c_m} \frac{1}{1 + \delta/(1 + \rho)} \quad (24)$$

Note that the electromechanical coupling factor δ is the ratio of the electrical damping of a short-circuited electromagnetic transducer, Φ^2/R_T , to the mechanical damping, c_m , and the factor $\delta/(1 + \rho)$ in Eq. (24) corresponds to the ratio of the electrical damping of the transducer terminated by the load resistance R to the mechanical damping.

3. Power and bandwidth analysis

3.1. Power analysis

The instantaneous harvested power is calculated as the electric power consumed by the load resistance as

$$P(t) = [\Phi \dot{x}(t)]^2 \frac{R}{(R + R_T)^2} \quad (25)$$

Substituting the steady-state solution $\dot{x}(t) = -a\omega \sin(\omega t - \psi)$ followed by taking the average over the period leads to the averaged harvested power given by

$$\bar{P} = \frac{\Phi^2 a^2 \omega^2}{2} \frac{R}{(R + R_T)^2} \quad (26)$$

The harvested power at the resonance peak is thus calculated as follows from Eq. (26) by evaluating it at the resonance peak point (ω_r, a_r) followed by applying Eqs. (19) and (11):

$$\begin{aligned} \bar{P}_r &= \frac{\Phi^2 a_r^2 \omega_r^2}{2} \frac{R}{(R + R_T)^2} \\ &= \frac{\Phi^2 m^2 u_a^2}{2 \left(c_m + \frac{\Phi^2}{R + R_T} \right)^2} \frac{R}{(R + R_T)^2} \\ &= \frac{m^2 u_a^2}{2c_m} \frac{\rho \delta}{(1 + \rho + \delta)^2} \end{aligned} \quad (27)$$

Eq. (27) states that the harvested power at the resonance peak is determined by the mass of the resonator, base-excitation magnitude, mechanical damping, electromechanical coupling factor, and load resistance, not by the resonance frequency. This means that the height of the resonance peak in the frequency-power curve is independent of the

stiffness of the resonator, whether it is linear or nonlinear, as pointed out in the literature [8, 27], as long as the values of the other parameters are the same.

From Eq. (27), the optimum load resistance that maximizes the harvested power at the resonance peak is derived in a dimensionless form as

$$\rho_{\text{opt}} = 1 + \delta \quad (28)$$

and thus the maximized power is

$$\bar{P}_{r,\text{opt}} = \frac{m^2 u_a^2}{8c_m} \frac{\delta}{1 + \delta} \leq \frac{m^2 u_a^2}{8c_m} \quad (29)$$

The upper bound of the harvested power is realized when the electromechanical coupling factor goes to infinity, and the upper bound increases for larger mass, larger input, and smaller mechanical damping, as in the linear case [2].

From Eq. (26), it is found that the same value of $a\omega$ gives the same harvested power. Therefore, the harvested power is constant on the hyperbola $a\omega=\text{const}$, which is hereafter called the iso-power curve in this paper. In this terminology, curve C2 is an iso-power curve passing through the tip of the resonance peak.

3.2. ν -power bandwidth

For a linear resonator, the bandwidth of its resonance peak is usually measured by the half-power bandwidth, which is defined as the range of frequencies for which the power is greater than half of its peak value. This is simply determined by taking a cross-section of the frequency response curve on the (ω, a) -plane with respect to a horizontal line at $1/\sqrt{2}$ of the peak value.

For nonlinear resonators, similar measures of the bandwidth are adopted in the literature. Ramlan et al. [27] discussed the harvested power for an energy harvester comprising hardening stiffness with cubic nonlinearity, and derived a closed-form representation of its half-power bandwidth, which was calculated in the same way as the linear resonator by taking a cross-section of the frequency-displacement curve with respect to $1/\sqrt{2}$ of the peak value. This method of calculation, however, can result in an overestimate of the bandwidth when the nonlinearity of the resonator is strong. Sebald et al. [28] studied the power and bandwidth of piezoelectric energy harvesters with cubic nonlinearity. They evaluated a half-power bandwidth by directly taking a cross-section of the power-frequency curve with respect to the half of the peak value, and normalizing it by taking a ratio with respect to the peak frequency. The same definition of the bandwidth can also be found in Cottone et al. [44] and Roy et al. [45].

In this study, a ν -power bandwidth is newly introduced as a straightforward extension of the half-power bandwidth, and is defined as the difference of the upper and lower frequencies at which the ratio of the power to its peak value is reduced to ν , where $0 < \nu < 1$. In the following, a formulation of the ν -power bandwidth and its graphical representation are given, and a further simplified formulation is approximately derived under the lightly damped condition.

At the intersection of the power-frequency curve with power level \bar{P}_ν , which is ν times the peak value \bar{P}_r , it holds that

$$\bar{P} = \bar{P}_\nu = \nu \bar{P}_r \quad (30)$$

Then, applying Eqs. (26) and (27) to Eq. (30) yields

$$a\omega = \sqrt{\nu} a_r \omega_r \quad (31)$$

Eq. (31) defines an iso-power curve C3 on (ω, a) -plane representing a boundary above which the harvested power is greater than ν times the maximum. Therefore, the intersection between C3 and the resonance curve bounds the ν -power band. More precisely, if the frequency response curve is a single-valued function of the frequency, as illustrated in Fig. 4 (a), the frequencies of the left and right intersections, which are respectively denoted by ω_1 and ω_2 in the figure, give the lower and upper boundaries, respectively. Whereas, if the frequency response curve has a multivalued region, as illustrated in Fig. 4 (b), the upper boundary is given by the jump-down frequency, which is approximately equal to the resonance frequency ω_r . Thus, a dimensionless form of the ν -power bandwidth, ν -PBW, is defined as follows by normalizing the difference of the boundary frequencies by the resonance frequency:

$$\nu\text{-PBW} = \begin{cases} (\omega_2 - \omega_1)/\omega_r & \text{(for single-valued frequency response)} \\ (\omega_r - \omega_1)/\omega_r & \text{(for multivalued frequency response)} \end{cases} \quad (32)$$

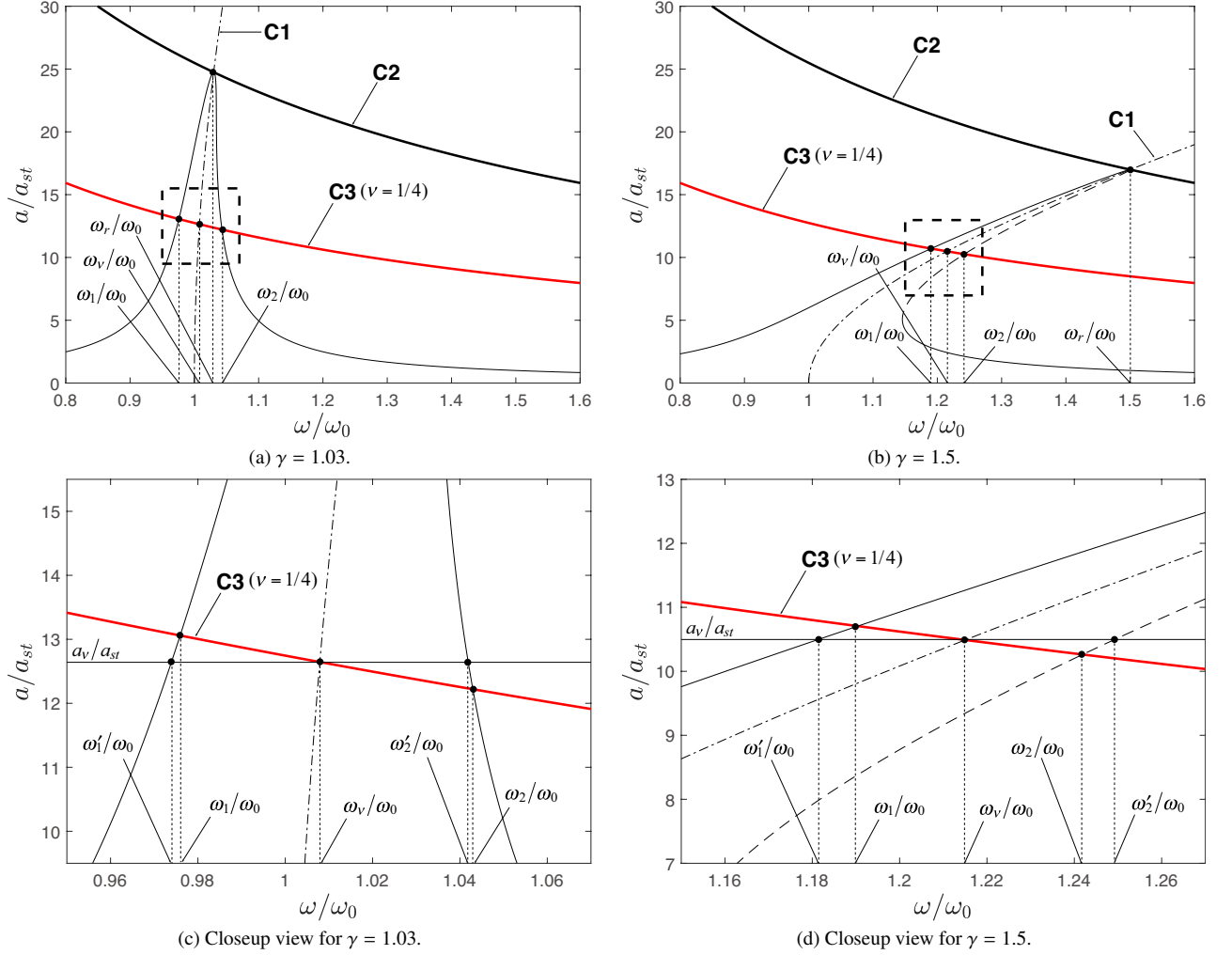


Figure 4: Calculation of the ν -power bandwidth from the intersection frequencies of the resonance curve and the iso-power curve C3 for $\nu=1/4$, for the case of single-valued frequency response ((a) and (c)), and the case of multivalued frequency response ((b) and (d)). The plots in (c) and (d) are the closeup view of the intersection shown in (a) and (b), respectively. Frequencies ω'_1 and ω'_2 are the approximation of the true intersection frequencies ω_1 and ω_2 given by Eq. (38). The center frequency $\omega_\nu = \omega_{\text{eq}}(a_\nu)$ is used to define ν -PBW''' as Eq. (40), a further approximation of the ν -power bandwidth, which is adopted in the successive sections to quantify the bandwidth.

In order to evaluate the ν -PBW given by Eq. (32), the intersection frequencies ω_1 and ω_2 have to be specified. These are derived by first eliminating ω from Eq. (31) by using Eq. (17) to get

$$\frac{1}{4} \left(\frac{m\mu_a}{K_{\text{eq}}(a)a} \right)^2 - \zeta_{\text{eq}}^2(a) = \left(\sqrt{\nu} \sqrt{\frac{m}{K_{\text{eq}}(a)} \frac{a_r \omega_r}{a}} - 1 \right)^2 \quad (33)$$

which is further rewritten by considering Eq. (19) as

$$\zeta_{\text{eq}}^2(a) \left[\left(\frac{a_r \omega_r}{a \omega_{\text{eq}}(a)} \right)^2 - 1 \right] = \left(\sqrt{\nu} \frac{a_r \omega_r}{a \omega_{\text{eq}}(a)} - 1 \right)^2 \quad (34)$$

and then solving Eq. (34) with respect to a , followed by substituting it into Eq. (17).

Instead, recalling the weak damping and resonance assumptions, i.e., $\zeta_{\text{eq}} = O(\varepsilon)$ and $a_r/a = O(1)$, and further assuming that the equivalent natural frequency for the supposed range of a is in the same order of the resonance frequency ,

i.e., $\omega_r/\omega_{\text{eq}}(a)=O(1)$, Eq. (34) reduces to

$$a\omega_{\text{eq}}(a) = \sqrt{\nu}a_r\omega_r \quad (35)$$

by evaluating the left-hand side negligibly small. Eq. (35) can be further divided into a system of equations composed of

$$a\omega = \sqrt{\nu}a_r\omega_r \quad (36)$$

which is again the equation of curve C3, and

$$\omega = \omega_{\text{eq}}(a) \quad (37)$$

which is the equation of curve C1 (the backbone curve). Hence, the ordinate value of the intersection of curves C1 and C3, which is denoted by a_ν , gives the solution of Eq. (35), i.e., an approximation of the solution of Eq. (34). By introducing this approximation, the approximate values of ω_1 and ω_2 , which are respectively denoted by ω'_1 and ω'_2 , are derived by evaluating Eq. (17) for $a=a_\nu$, and then applying Eqs. (19) and (35) as

$$\omega'_1, \omega'_2 = \omega_{\text{eq}}(a_\nu) \left[1 \mp \zeta_{\text{eq}}(a_\nu) \sqrt{\frac{1-\nu}{\nu}} \right] \quad (38)$$

both of which are also depicted in Figs. 4 (c) and (d). Therefore, an approximated dimensionless ν -power bandwidth, ν - PBW' , is derived as follows by replacing ω_1 and ω_2 in Eq. (32) by ω'_1 and ω'_2 , and substituting Eq. (38):

$$\nu\text{-}PBW' = \begin{cases} 2\zeta_{\text{eq}}(a_\nu) \sqrt{\frac{1-\nu}{\nu}} \frac{\omega_{\text{eq}}(a_\nu)}{\omega_r} & \text{(for single-valued frequency response)} \\ 1 - \left(1 - \zeta_{\text{eq}}(a_\nu) \sqrt{\frac{1-\nu}{\nu}} \right) \frac{\omega_{\text{eq}}(a_\nu)}{\omega_r} & \text{(for multivalued frequency response)} \end{cases} \quad (39)$$

Eq. (39) gives a theoretical basis of how a resonance band much wider than that of a linear resonator is accomplished when the frequency response is multivalued. This can be understood by considering that the dimensionless ν -power bandwidth of a linear resonator with a damping ratio of $\zeta=O(\varepsilon)$ is derived as $2\zeta \sqrt{(1-\nu)}/\nu=O(\varepsilon)$, whereas that of the nonlinear resonator with a multivalued frequency response is evaluated from Eq. (39) as $O(1)$ because $1-\omega_{\text{eq}}(a_\nu)/\omega_r=O(1)$. In this case, the dimensionless ν -power bandwidth gives the allowable rate of the descent of the excitation frequency from the resonance frequency to guarantee that the harvested power is at least ν times the maximum value, given the specific harvester design and excitation amplitude.

Notably, multivalued resonance emerges when the nonlinearity of the restoring force is sufficiently strong, excitation is sufficiently large, and damping is sufficiently low. These conditions were explicitly formulated by Malatkar and Nayfeh [46] in the case of the Duffing oscillator using the Sylvester resultant. A straightforward extension of the same mathematical treatment would be possible, leading to similar explicit conditions even in the case of the higher order nonlinearity.

For a more simplified formulation, the second row of Eq. (39) is further reduced, by considering $\zeta_{\text{eq}}(a_\nu)=O(\varepsilon)$, to

$$\nu\text{-}PBW'' = 1 - \frac{\omega_{\text{eq}}(a_\nu)}{\omega_r} \quad (40)$$

which is analogous to the approximation presented by Ramlan et al. [27]. The above definition of ν - PBW'' is adopted hereafter to quantify the bandwidth.

Recalling that $(\omega_{\text{eq}}(a_\nu), a_\nu)$ is the intersection of curves C1 and C3, and that backbone curve C1 is bounded by four lines, $\omega=\omega_0$, $\omega=\omega_r$, $a=0$, and $a=a_r$, it is concluded that $\omega_{\text{eq}}(a_\nu) > \max(\omega_0, \sqrt{\nu}\omega_r) = \max(\omega_r/\gamma, \sqrt{\nu}\omega_r)$. Therefore, the dimensionless bandwidth ν - PBW'' is bounded from above as

$$\nu\text{-}PBW'' < \min\left(1 - \frac{1}{\gamma}, 1 - \sqrt{\nu}\right) \quad (41)$$

For demonstrative purposes, the ν -power bandwidth of the resonators with odd-power nonlinearity is being calculated. This is done by first evaluating Eq. (35) for the backbone curve specified by Eq. (B.11), leading to

$$\alpha \left[1 + (\gamma^2 - 1)\alpha^n \right] = \nu\gamma^2 \quad (42)$$

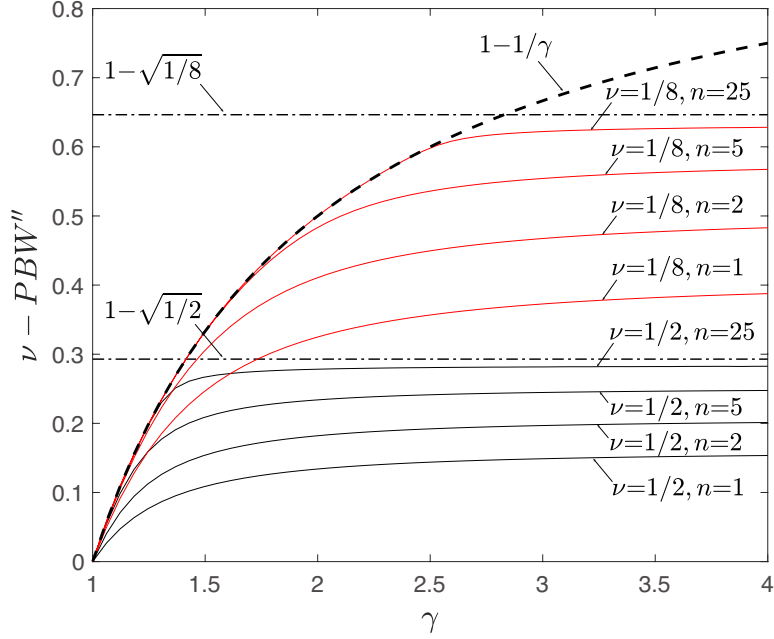


Figure 5: The dependency of the ν -power bandwidth ν - PBW'' on γ , the ratio of the resonance frequency to the linear natural frequency, and n , the order of the odd-power nonlinearity, for $\nu=1/2$ (plotted in thin black lines) and $1/8$ (plotted in thin red lines). The bold dashed black line shows the curve $1-1/\gamma$, and the thin chained black lines show $1-\sqrt{\nu}$. The plot indicates that the bandwidth becomes broader as the value of γ increases, and exhibits saturation at the value given by Eq. (44). Moreover, the bandwidth approaches its upper bound given by Eq. (41) as the order of the nonlinearity increases. (For interpretation of the references to color in this figure legend, the reader is referred to the web version of this article.)

where α is defined as $\alpha=(a/a_r)^2$, and then solving Eq. (42) with respect to α to obtain $a_\nu=\sqrt{\alpha_\nu}a_r$, where α_ν is the solution of Eq. (42). The ν -power bandwidth is derived by evaluating Eq. (40) for the resulting a_ν , or directly derived from

$$\nu$$
- $PBW'' = 1 - \sqrt{\frac{\nu}{\alpha_\nu}} \quad (43)$

which is obtained by rewriting Eq. (40) using Eq. (35).

Fig. 5 shows the ν - PBW'' of the harvesters with different orders of nonlinearity, $n=1, 2, 5$, and 25 , as a function of γ , for $\nu=1/2$ and $1/8$. It is obvious that every curve plotted in Fig. 5 exhibits saturation at a certain value of the bandwidth, which is calculated from Eqs. (42) and (43) by taking the limit $\gamma \rightarrow \infty$ leading to

$$\nu$$
- $PBW'' \Big|_{\gamma \rightarrow \infty} = 1 - \nu^{n/(2n+2)} \quad (44)$

This equation suggests that as the order of the nonlinearity becomes larger the saturation value approaches $1-\sqrt{\nu}$. Moreover, Fig. 5 indicates that the value of ν - PBW'' also comes closer to $1-1/\gamma$ in the region where γ is small. From these findings, it is concluded that the more deeply the backbone curve bends, the closer the bandwidth is to its upper bound described by Eq. (41).

3.3. Dependence of power-bandwidth performance on coupling strength and load resistance

The impact of the electromechanical coupling factor and load resistance on the power-bandwidth performance of the harvester is particularly focused on in this section. Given the design of the mechanical part of the resonator, the peak power given by Eq. (27) and the equations of curves C2 and C3 given by Eqs. (24) and (31) are respectively rearranged as

$$\bar{P}_r(\delta, \lambda) = \frac{m^2 u_a^2}{2c_m} \frac{\delta \lambda}{(1+\delta)(1+\lambda)^2} \quad (45)$$

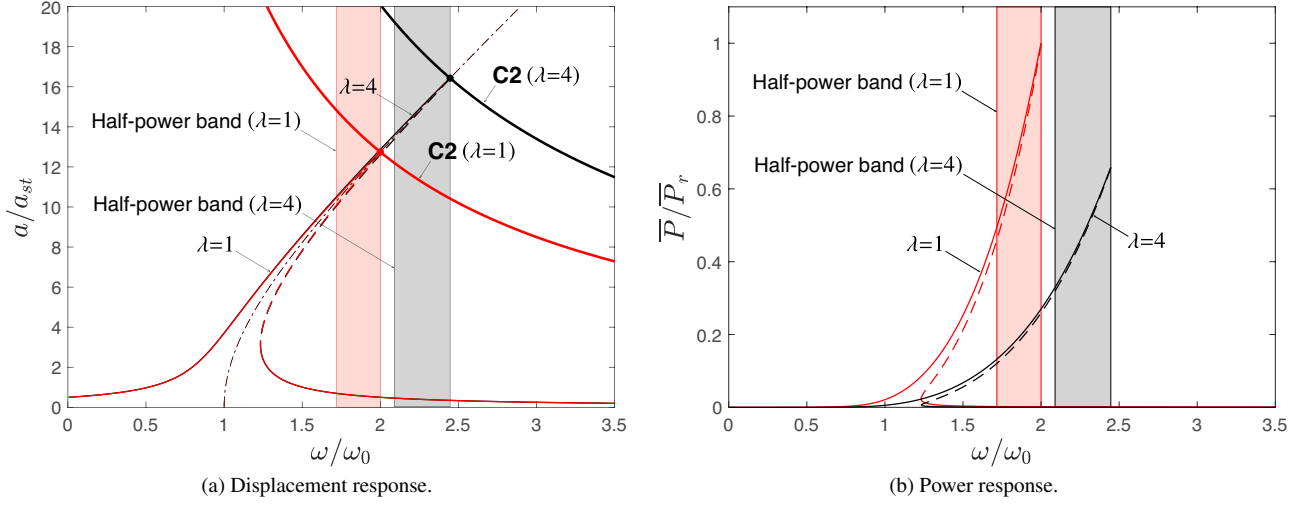


Figure 6: Displacement-frequency response (a) and power-frequency response (b) for the case of optimal load (plotted in thin solid red lines) and the case of a larger load, i.e., four times the optimal load, (plotted in thin solid black lines). The corresponding C2 curves and the 1/2-power bands (half-power bands) are depicted by bold solid lines and colored rectangular areas, respectively. The plots indicate that by increasing the load resistance the half-power band is slightly widened, but in return, the harvested peak power is significantly reduced as the load impedance is mismatched. (For interpretation of the references to color in this figure legend, the reader is referred to the web version of this article.)

$$C2(\delta, \lambda): \quad a\omega = \frac{mu_a}{c_m} \frac{\lambda + 1/(1 + \delta)}{1 + \lambda} \quad (46)$$

and

$$C3(\delta, \lambda): \quad a\omega = \sqrt{\nu} \frac{mu_a}{c_m} \frac{\lambda + 1/(1 + \delta)}{1 + \lambda} \quad (47)$$

by parametrizing the load resistance as $\rho = \lambda \rho_{\text{opt}} = \lambda(1 + \delta)$.

First, let us consider the effect of the electromechanical coupling strength on the harvested power and ν -power bandwidth. As $\bar{P}_r(\delta, \lambda)/\bar{P}_r(\infty, \lambda) = \delta/(1 + \delta)$, derived from Eq. (45), a strong coupling, e.g., $\delta > 10$, can provide power sufficiently close to its maximum, i.e., the power for the infinite coupling case. Furthermore, since the right-hand sides of Eqs. (46) and (47) are approximated by $mu_a \lambda / [c_m(1 + \lambda)]$ and $\sqrt{\nu} mu_a \lambda / [c_m(1 + \lambda)]$, respectively, if $1/(1 + \delta) \ll \lambda$, which is true when the coupling is strong and $\lambda \geq 1$, the resonance peak point as well as the ν -power bandwidth are sufficiently close to those for the infinite coupling case. These findings suggest that, if one achieves a design of the transducer with a certain level of coupling strength, further pursuit of stronger coupling is almost meaningless, and thus, one can safely assume $\delta \rightarrow \infty$ when evaluating the power-bandwidth performance.

Next, the effect of the load resistance on the power-bandwidth performance is detailed. Fig. 6 shows an illustrative example in which the displacement responses and power responses are plotted along with their 1/2-power bands for the optimal load case ($\lambda = 1$), and a larger load case ($\lambda = 4$) aiming to shift the peak frequency higher. It is apparent from Fig. 6 (a) that, for the case with $\lambda = 4$ (thin solid black line), a peak frequency 1.22 times higher than the optimal load case (thin solid red line) is achieved, and consequently, the half-power band is slightly widened as depicted in the figure by colored areas. However, at the cost of the small gain in the bandwidth, the harvested peak power is significantly reduced since the load impedance is mismatched.

The dependency of the peak power performance on the load resistance is characterized by taking the ratio of the power given by Eq. (45) to the power with the optimal load leading to the following expression:

$$\frac{\bar{P}_r(\delta, \lambda)}{\bar{P}_r(\delta, 1)} = \frac{4\lambda}{(1 + \lambda)^2} \quad (48)$$

Apparently, the optimal value of λ is one. Meanwhile, the dependency of the resonance bandwidth on λ can be clarified by evaluating the ratio of the ν -power bandwidth to that for the optimal load case. Fig. 7 shows the power

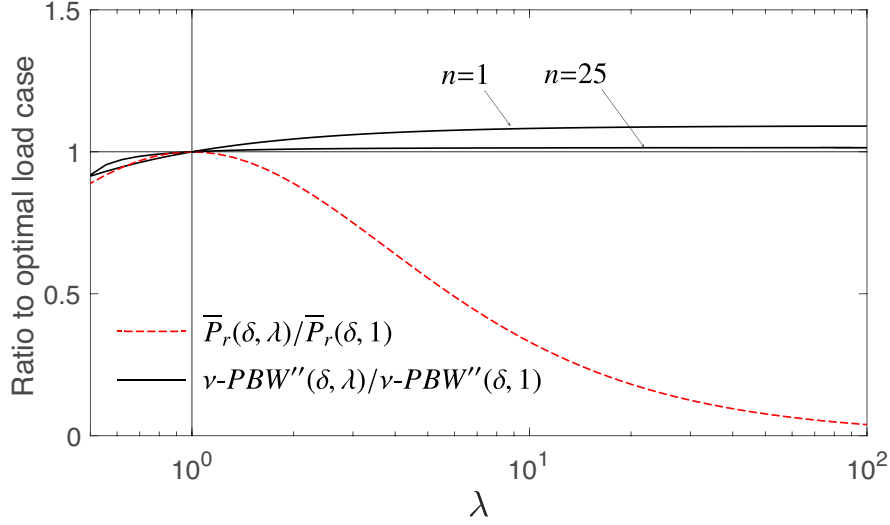


Figure 7: The ratio of the power to its optimal load case given by Eq. (48) (plotted in dashed red line), and the ratio of the ν -power bandwidth to its optimal load case for $\nu=1/2$, $\delta=50$, and $n=1, 25$ (plotted in solid black lines). It is concluded from the figure that setting the load resistance higher than its optimal value may slightly increase the bandwidth, but not be beneficial enough to sacrifice the power performance. (For interpretation of the references to color in this figure legend, the reader is referred to the web version of this article.)

ratio given by Eq. (48) and the bandwidth ratio ν - $PBW''(\delta, \lambda)/\nu$ - $PBW''(\delta, 1)$ for $\nu=1/2$ and $\delta=50$. It is evident from this figure that setting a load resistance higher than its optimal value may slightly increase the bandwidth, but is not recommended because the gain in the bandwidth is outweighed by the loss of the power performance. For this reason, the optimal load resistance is assumed in the next section when considering the design scheme.

4. Power-bandwidth design

4.1. Problem statement and assumptions

In this section, the process of designing a nonlinear vibration energy harvester with a hardening restoring force to achieve its optimal power-bandwidth performance under the given design requirements is presented. In the design of vibration energy harvesters, the frequency characteristics of the resonator are required to match those of the vibration source to maintain the resonator responding in resonance. For nonlinear harvesters, the vibration source is usually assumed to be sinusoidal with a slowly or occasionally changing frequency and amplitude. Thus, the resonator's bandwidth is required to cover the prospective range of such a fluctuation in the frequency and amplitude of the vibration source. The size of the harvester is another critical design requirement because it limits the allowable stroke of the resonator as well as its effective mass.

Therefore, the design problem addressed in this section is stated as follows: for a given range of the fluctuation in the frequency and amplitude of the base acceleration, to design a nonlinear harvester with the maximum ν -power bandwidth for the predetermined device size requirement.

The following assumptions are made to quantify and simplify the design problem:

- The frequency ω and amplitude u_a of the base acceleration fluctuate independently, within the ranges of $[\omega^{lb}, \omega^{ub}]$ and $[u_a^{lb}, u_a^{ub}]$, respectively.
- The mass m of the resonator as well as its stroke limit L are predetermined such that they meet the device size requirement.
- The value of the mechanical damping c_m is predetermined. This is a reasonable assumption when the resonator's structure is carefully designed such that the mechanical damping ratio ζ is sufficiently small, e.g., less than 0.01,

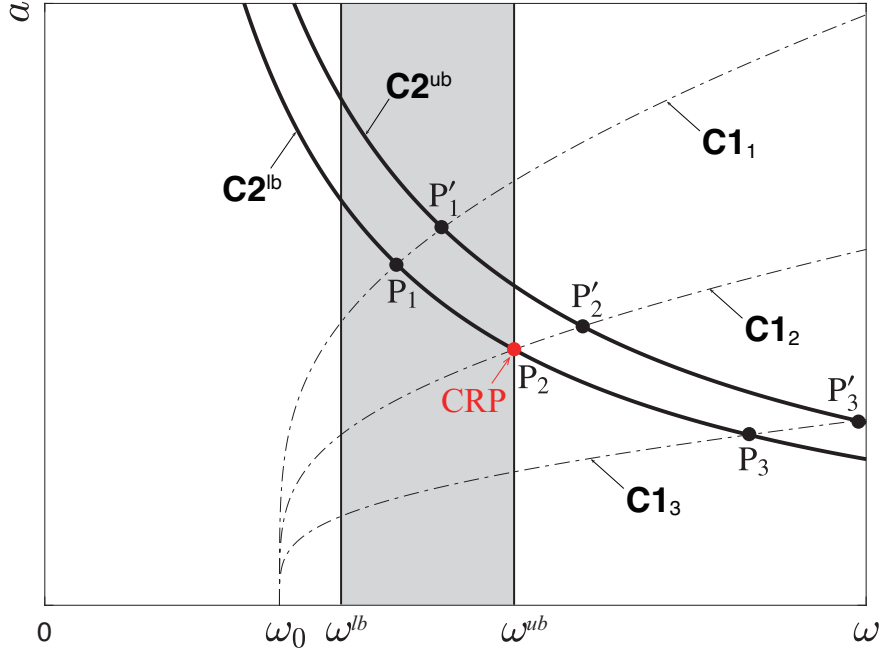


Figure 8: Diagram illustrating the assumed excitation conditions on the (ω, a) -plane. Curves $C2^{lb}$ and $C2^{ub}$ (plotted in bold black lines) are the C2 curves for the excitation amplitudes of lower bound u_a^{lb} and upper bound u_a^{ub} , respectively. The gray area depicts the excitation frequency band bounded by $\omega=\omega^{lb}$ and $\omega=\omega^{ub}$. Curves $C1_1$, $C1_2$, and $C1_3$ are the backbone curves for different strengths of nonlinearity, i.e., $n=5$ with different values of β . The CRP is the intersection of $C2^{lb}$ and line $\omega=\omega^{ub}$. In the illustrated case, backbone curve $C1_2$ is the one that conforms to the CRP.

at the operating frequency. Then the value of c_m can be estimated as $c_m=2\zeta m\omega_{rep}$, where $\omega_{rep}=(\omega^{lb}+\omega^{ub})/2$ is the representative operating frequency.

- The electromechanical coupling is strong enough, e.g., $\delta>10$, and the load resistance is set to be optimal.

As mentioned in the introduction, the design of nonlinear vibration energy harvesters is always accompanied with the problem of coexisting multiple solutions. This is critical particularly in the situation assumed above, in which the frequency and magnitude of the vibration source may fluctuate, because the response of the nonlinear resonator easily drops to the low-energy branch, which generates almost no power. This difficulty, however, is expected to be overcome by introducing some additional techniques that work to maintain the resonator's response in the highest-energy branch [28, 31, 32, 33, 34, 35, 36, 37, 38, 39]. Therefore, in this study, the problem of coexisting multiple solutions is excluded from consideration as it can be solved separately.

4.2. Design scheme

Fig. 8 shows a diagram that illustrates the assumed conditions on the (ω, a) -plane. Curves $C2^{lb}$ and $C2^{ub}$ are the C2 curves for the excitation amplitudes of lower bound u_a^{lb} and upper bound u_a^{ub} , respectively. The excitation frequency band bounded by $\omega=\omega^{lb}$ and $\omega=\omega^{ub}$ is depicted by the gray area. Given these conditions, it is necessary to guarantee the existence of a high energy branch for all possible combinations of excitation frequencies and amplitudes to exploit the advantages of nonlinear resonators.

The design scheme begins with determining the location of a “critical” resonance point on the (ω, a) -plane. Let us suppose the resonators with a specific nonlinearity. Curves $C1_1$, $C1_2$, and $C1_3$ in Fig. 8 are the backbone curves of resonators with different strengths of nonlinearity, i.e., weak, medium, and strong, respectively. The intersection between one of these C1 curves and $C2^{lb}$, depicted by P_n ($n=1, 2, 3$), is the resonance point for the excitation with the lowest level, while the intersection depicted by P'_n is the resonance point for the highest level. This means that the segment of $C1_n$ bounded by P_n and P'_n forms the set of resonance points for all the possible levels of excitation.

Considering the fact that the right-end of the high energy branch is terminated by the resonance point, it is thus necessary that all the possible resonance points must be located right outside of the excitation frequency band $[\omega^{\text{lb}}, \omega^{\text{ub}}]$ to guarantee the existence of the high energy branch inside. Therefore, it is concluded that the case in which the resonance point for the lowest level of excitation is located on the upper boundary of the excitation frequency band is critical to meet this requirement. More specifically, this resonance point is the intersection of $C2^{\text{lb}}$ and line $\omega=\omega^{\text{ub}}$, which hereafter will be called the CRP.

In determining the CRP, it would be useful to mention a few points. First, the assumptions regarding the excitation frequency and amplitude may not always be satisfied in practical situations, even if they are set very conservatively. The excitation amplitude may accidentally become smaller than the lower limit u_a^{lb} , or the excitation frequency may exceed the upper limit ω^{ub} . If this happens, one has to admit the case that there no longer is the high energy branch for some excitation frequencies, and the only thing one can do is to wait for the excitation to return to the predetermined range of frequency and amplitude. Second, according to Eq. (46), curve C2 depends not only on the given excitation condition but also on the design parameters, namely, the mass m and mechanical damping c_m related to the mechanical design of the resonator, electromechanical coupling factor δ dependent on the transducer design, and load resistance magnitude λ to be selected optimal. As the selection of the CRP relies on these design parameters, which should be readjusted during the iteration process of the design work, the location of the CRP should also be adjusted during the design process. Third, the response amplitude for all possible excitation conditions should be smaller than the stroke limit L . This implies that the CRP must be below the line $a=L$ with an appropriate margin. If the CRP once determined from curve $C2^{\text{lb}}$ and line $\omega=\omega^{\text{ub}}$ unfortunately exceeds the stroke limit, it may be worth considering to expand the stroke limit by easing the device size requirement in order to exploit the harvester's potential performance.

Once the CRP is appropriately selected, what follows next is the determination of the force-displacement relationship of the mechanical spring of the resonator that provides the optimal nonlinearity for the power generation. This is done by maximizing the ν -power bandwidth while keeping the resonance peak point at the CRP by selecting an appropriate value of γ . This is equivalent to setting an appropriate value of the linear natural frequency ω_0 , such that the harvester can tolerate the ω^{lb} as low as possible. More concrete and quantitative discussions will be presented in the next section.

4.3. Design study for harvesters with odd-power nonlinearity

A design study is performed in this section for a harvester with odd-power nonlinearity for given design requirements. Suppose that the excitation conditions ω^{lb} , ω^{ub} , u_a^{lb} , and u_a^{ub} are given, and the parameters m , c_m , L are predetermined. Then, the CRP is reasonably determined from curve $C2^{\text{lb}}$ and line $\omega=\omega^{\text{ub}}$.

The nonlinear restoring force function is determined so that its backbone curve passes through the CRP. The set of such functions is formulated by using Eqs. (B.1) and (B.9), resulting in

$$f(x) = \frac{k_{\text{CRP}}a_{\text{CRP}}}{\gamma^2} \left[\left(\frac{x}{a_{\text{CRP}}} \right) + \frac{\gamma^2 - 1}{A_n} \left(\frac{x}{a_{\text{CRP}}} \right)^{2n+1} \right] \quad (49)$$

where $k_{\text{CRP}}=m\omega_{\text{CRP}}^2$, and $(\omega_{\text{CRP}}, a_{\text{CRP}})$ is the location of the CRP. The concrete shape of the force function $f(x)$ is finalized by choosing γ for the assumed value of n , such that the ν -power bandwidth is maximized. From Fig. 5, it is evident that a larger γ results in a wider bandwidth, hence the optimal value of γ is infinite, which is however a meaningless conclusion. On the other hand, setting the value of γ too large should be avoided because it requires that the backbone curve be more deeply bent, which means more apparent hardening of the nonlinear spring, which could lead to difficulties in designing the spring mechanism. Considering that every curve shown Fig. 5 exhibits saturation at the value of the bandwidth given by Eq. (44), one reasonable choice is to select the value of γ that achieves a bandwidth slightly smaller than its saturated value, e.g., 90% of it.

The resultant values of γ for $\nu=1/2$ and $n=1, 2, 5, 25$, and the resultant values of ν -PBW'' are listed in Table 1. It can be seen from the table that a higher order nonlinearity achieves a wider bandwidth with smaller values of γ . Note that selecting the value of γ means selecting the linear natural frequency ω_0 because the resonance frequency is already fixed by the location of the CRP. The force-displacement curves of the resultant $f(x)$ and the resonance curves for $n=1$ and 25 are plotted in Fig. 9. It is shown that a higher order nonlinearity can achieve a wider bandwidth with higher values of the linear natural frequency.

Table 1: Results of the design study; the resultant values of γ and ν -PBW'' for $\nu=1/2$ and $n=1, 2, 5, 25$ are listed. It is found that a higher order of nonlinearity achieves wider bandwidth with smaller values of γ .

n	1	2	5	25
γ	2.45	2.14	1.75	1.39
$1/2$ -PBW''	0.143	0.186	0.226	0.255

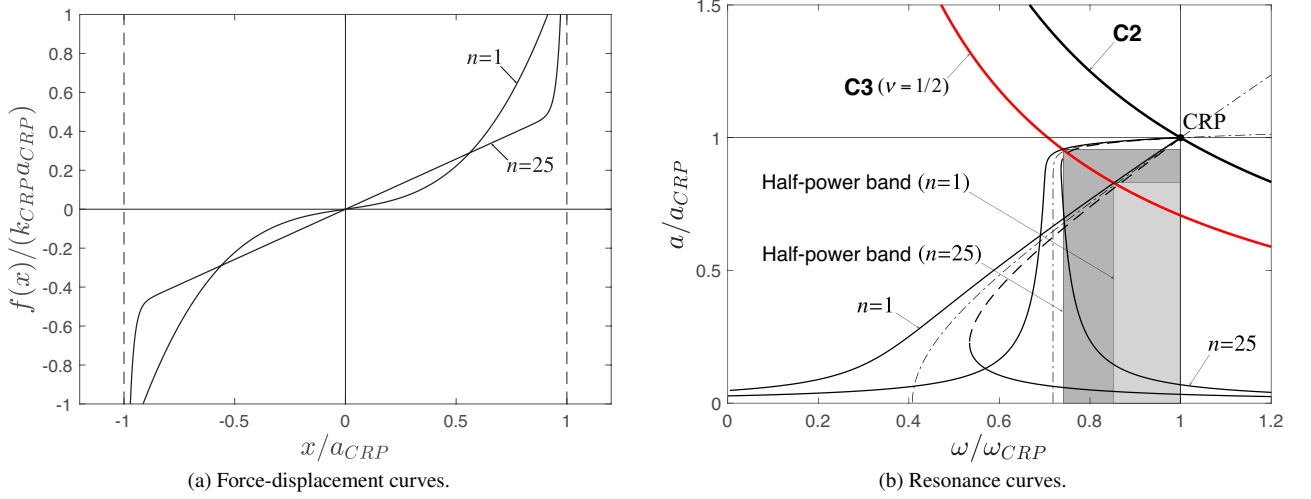


Figure 9: Results of the design example for $n=1$ and 25 ; (a) force-displacement curves given by Eq. (49), and (b) frequency-displacement curves. Both plots are normalized by the values on the CRP. In (b), curves C2 and C3 for $\nu=1/2$ are also plotted. Light gray and dark gray areas are the $1/2$ -power bands (half-power bands) for $n=1$ and 25 , respectively. It is shown that a higher order of nonlinearity achieves a wider bandwidth with smaller values of γ , i.e., higher values of the linear natural frequency.

An actual nonlinear resonator may not have an exact odd-power nonlinearity. Even in such a case, the design procedure proposed in Sections 4.2 and 4.3 can effectively be used by making a diagram corresponding to Fig. 5 for the given class of nonlinearity. Otherwise, if the force-displacement relationship is reasonably approximated by an odd-power function, the above discussion can directly be applied.

Moreover, to implement the proposed design scheme, it is necessary to design and fabricate a spring that has a resonance point at the predetermined CRP, as described in Eq. (49). Currently, the trial-and-error approach is realistic, and the synthesis of a spring with desired characteristics is a challenge. One possibility is to take a synthesis approach proposed by Zou et al. [47, 48], in which a cam-like mechanism is used to achieve arbitrary restoring force characteristics.

5. Conclusions

In this paper, a theoretical foundation for designing the power and bandwidth performance of nonlinear vibration energy harvesters was established based on analytical formulae derived from the first-order steady-state solution of the mathematical model of an electromagnetic harvester with a hardening resonator.

First, a graphical approach was proposed to provide a clear understanding of how the design parameters and excitation conditions determine the location of the resonance peak point on the frequency-displacement curve. It was revealed that the resonance peak point is located at the intersection between an iso-power curve and the backbone curve, the former of which is determined by the excitation magnitude, mass, and total damping, whereas the latter by the equivalent stiffness of the nonlinear restoring force. Then, a ν -power bandwidth, a generalized version of the half-power bandwidth, was defined, and its approximate formulation was presented. Based on the findings of the

parameter study on the ν -power bandwidth, a design scheme that aims to optimize the ν -power bandwidth under assumed design requirement was developed. The proposed scheme begins with specifying the CRP, the resonance point that guarantees the existence of the high-energy branch of the solution under possible variations of the excitation, followed by determining the linear natural frequency that makes the ν -power bandwidth as large as reasonably possible. Finally, a design study for a harvester with odd-power nonlinearity was performed, and it was found that a higher order nonlinearity is advantageous because it can achieve a wider bandwidth with higher values of the linear natural frequency.

In summary, this work provides a rational way to maximize the power-bandwidth performance of a nonlinear vibration energy harvester while incorporating various design requirements. Because this work first assumes that the resonator can maintain its high-energy response by introducing some extra methodologies, the stability margin of the high-energy solution is beyond the scope of this work. Needless to say, a large stability margin helps maintain the high-energy solution under disturbances. As the parameters and functions obtained through the proposed design scheme may also have significant influences on the stability margin, there is a need to elucidate these influences and investigate a design methodology that maximizes the bandwidth while ensuring the stability margin, which would be one of future works to be addressed. In addition, experimental verification and extension of this study to other types of nonlinearity (softening, reversible, etc.) should be addressed in future study.

Acknowledgements

This work was supported in part by JSPS KAKENHI Grant Number 21K03936. The author thanks Editage (www.editage.com) for English language editing.

Appendix A. The order evaluation of the right-hand side of Eq. (8)

Let us suppose that $m\omega^2$, the amplitude of the inertial force acting on the mass of the harvester, is $O(1)$. If the harvester is operated in the primary resonance condition, then mu_a , the amplitude of the excitation force, should be $O(\varepsilon)$ because it is much smaller than $m\omega^2$. Therefore, the third term on the right-hand side of Eq. (8) is $O(\varepsilon)$. Also, since the inertial force $-m\omega^2 \cos \theta$ and restoring force $f(a \cos \theta)$ almost balance each other during the resonance, it can be assumed $-m\omega^2 \cos \theta + f(a \cos \theta) = O(\varepsilon)$. This means that the first term on the right-hand side of Eq. (8) is $O(\varepsilon)$. In addition, if the mechanical and electrical damping of the harvester is light, the second term is also assumed to be $O(\varepsilon)$. Therefore, it can be concluded that the entire right-hand side of Eq. (8) is $O(\varepsilon)$.

Appendix B. Resonators with odd-power nonlinearity

For concrete examples provided in this paper, the following class of nonlinear restoring force is assumed:

$$f(x) = k_0 (x + \beta x^{2n+1}) \quad (\text{B.1})$$

where $\beta > 0$, and n is a positive integer. The equivalent stiffness is calculated as

$$\begin{aligned} K_{\text{eq}}(a) &= k_0 \left[1 + \frac{\beta}{\pi a} \int_0^{2\pi} (a \cos \theta)^{2n+1} \cos \theta d\theta \right] \\ &= k_0 (1 + \beta A_n a^{2n}) \end{aligned} \quad (\text{B.2})$$

where

$$A_n = \frac{(2n+2)!}{2^{2n+1}(n+1)!(n+1)!} \quad (\text{B.3})$$

For instance, for $n = 1$ (Duffing resonator),

$$K_{\text{eq}}(a) = k_0 \left(1 + \frac{3}{4} \beta a^2 \right) \quad (\text{B.4})$$

for $n = 2$,

$$K_{\text{eq}}(a) = k_0 \left(1 + \frac{5}{8} \beta a^4 \right) \quad (\text{B.5})$$

for $n = 5$,

$$K_{\text{eq}}(a) = k_0 \left(1 + \frac{231}{512} \beta a^{10} \right) \quad (\text{B.6})$$

and for $n = 25$,

$$K_{\text{eq}}(a) = k_0 \left(1 + \frac{7934696527169663}{36028797018963968} \beta a^{50} \right) \quad (\text{B.7})$$

Let us suppose that the resonance peak point is located at (ω_r, a_r) , and let $\omega_r = \gamma \omega_0$, where $\gamma > 1$ is a positive number of $O(1)$. Then, it is required from Eqs. (20) and (B.2) that

$$K_{\text{eq}}(a_r) = k_0 \left(1 + \beta A_n a_r^{2n} \right) = m \omega_r^2 = m \gamma^2 \omega_0^2 \quad (\text{B.8})$$

From Eq. (B.8), and recalling that $\omega_0 = \sqrt{k_0/m}$, the parameter β is derived as

$$\beta = \frac{\gamma^2 - 1}{A_n a_r^{2n}} \quad (\text{B.9})$$

Substituting this into Eq. (B.2) gives

$$K_{\text{eq}}(a) = k_0 \left[1 + (\gamma^2 - 1) \left(\frac{a}{a_r} \right)^{2n} \right] \quad (\text{B.10})$$

and the corresponding backbone curve is

$$\omega_{\text{eq}}(a) = \sqrt{1 + (\gamma^2 - 1) \left(\frac{a}{a_r} \right)^{2n}} \omega_0 \quad (\text{B.11})$$

The force-displacement curves given by Eqs. (B.1) and (B.9) for various values of n are plotted in Fig. B.1 (a) with $\gamma=2$. Fig. B.1 (b) displays the shapes of the corresponding backbone curves. The case for $n=1$ is the Duffing resonator. A larger n gives a more distinct bend to both the force-displacement curve and backbone curve that converge to those of a spring with rigid stoppers symmetrically placed at $x = \pm a_r$.

References

- [1] C. Williams, R. Yates, Analysis of a micro-electric generator for microsystems, in: Proceedings of the International Solid-State Sensors and Actuators Conference - TRANSDUCERS '95, vol. 1, 369–372, doi:10.1109/SENSOR.1995.717207, 1995.
- [2] N. G. Stephen, On energy harvesting from ambient vibration, Journal of Sound and Vibration 293 (1-2) (2006) 409–425, doi: 10.1016/j.jsv.2005.10.003.
- [3] J. M. Renno, M. F. Daqaq, D. J. Inman, On the optimal energy harvesting from a vibration source, Journal of Sound and Vibration 320 (1) (2009) 386–405, doi:10.1016/j.jsv.2008.07.029.
- [4] L. Tang, Y. Yang, C. K. Soh, Toward broadband vibration-based energy harvesting, Journal of Intelligent Material Systems and Structures 21 (18) (2010) 1867–1897, doi:10.1177/1045389X10390249.
- [5] D. Zhu, M. J. Tudor, S. P. Beeby, Strategies for increasing the operating frequency range of vibration energy harvesters: a review, Measurement Science and Technology 21 (022001) (2010) 1–29.
- [6] R. L. Harnes, K. W. Wang, A review of the recent research on vibration energy harvesting via bistable systems, Smart Materials and Structures 22 (2) (2013) 023001, doi:10.1088/0964-1726/22/2/023001.
- [7] S. P. Pellegrini, N. Tolou, M. Schenk, J. L. Herder, Bistable vibration energy harvesters: A review, Journal of Intelligent Material Systems and Structures 24 (11) (2013) 1303–1312, doi:10.1177/1045389X12444940.
- [8] M. F. Daqaq, R. Masana, A. Erturk, D. Dane Quinn, On the role of nonlinearities in vibratory energy harvesting: A critical review and discussion, Applied Mechanics Reviews 66 (4) (2014) 040801, doi:10.1115/1.4026278.
- [9] Y. Jia, Review of nonlinear vibration energy harvesting: Duffing, bistability, parametric, stochastic and others, Journal of Intelligent Material Systems and Structures 31 (7) (2020) 921–944, doi:10.1177/1045389X20905989.
- [10] M. S. M. Soliman, E. M. Abdel-Rahman, E. F. El-Saadany, R. R. Mansour, A wideband vibration-based energy harvester, Journal of Micromechanics and Microengineering 18 (11) (2008) 115021.

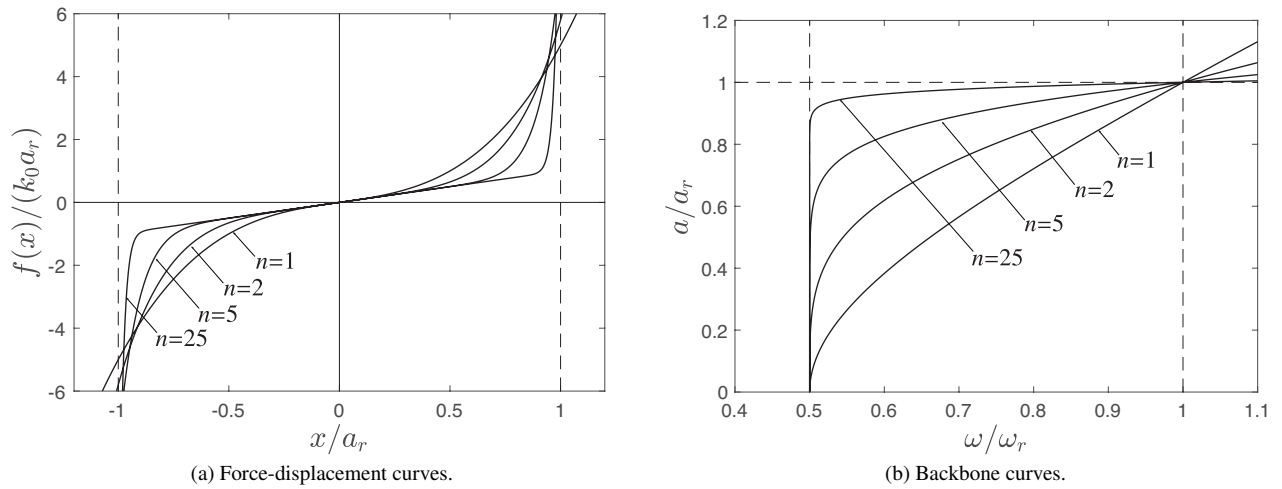


Figure B.1: Characteristics of resonators with odd-power nonlinearity ($n=1, 2, 5, 25$) for the case of $\gamma=2$; (a) force-displacement curves, and (b) backbone curves. The case for $n=1$ is the Duffing resonator. A larger n gives a more distinct bend to both the force-displacement curve and backbone curve that converge to those of a spring with rigid stoppers symmetrically placed at $x=\pm a_r$.

- [11] B. Mann, N. Sims, Energy harvesting from the nonlinear oscillations of magnetic levitation, *Journal of Sound and Vibration* 319 (1-2) (2009) 515 – 530, doi:10.1016/j.jsv.2008.06.011.
- [12] S. C. Stanton, C. C. McGehee, B. P. Mann, Reversible hysteresis for broadband magnetopiezoelectric energy harvesting, *Applied Physics Letters* 95 (17) 174103, doi:10.1063/1.3253710.
- [13] M. A. Karami, D. J. Inman, Nonlinear hybrid energy harvesting utilizing a piezo-magneto-elastic spring, in: *Proceedings of SPIE*, vol. 7643, 76430U, 2010.
- [14] D. D. Quinn, A. L. Triplett, L. A. Bergman, A. F. Vakakis, Comparing linear and essentially nonlinear vibration-based energy harvesting, *Journal of Vibration and Acoustics* 133 (1), doi:10.1115/1.4002782.
- [15] Y. Jin, S. Hou, T. Yang, Cascaded essential nonlinearities for enhanced vibration suppression and energy harvesting, *Nonlinear Dynamics* 103 (2021) 1427–1438, doi:10.1007/s11071-020-06165-6.
- [16] J. Margielewicz, D. Gąska, G. Litak, P. Wolszczak, D. Yurchenko, Nonlinear dynamics of a new energy harvesting system with quasi-zero stiffness, *Applied Energy* 307 (2022) 118159, doi:10.1016/j.apenergy.2021.118159.
- [17] A. Erturk, J. Hoffmann, D. J. Inman, A piezomagnetoelastic structure for broadband vibration energy harvesting, *Applied Physics Letters* 94 (25) 254102, doi:10.1063/1.3159815.
- [18] F. Cottone, H. Vocca, L. Gammaitoni, Nonlinear energy harvesting, *Physics Review Letters* 102 (2009) 080601, doi:10.1103/PhysRevLett.102.080601.
- [19] M. Ferrari, V. Ferrari, M. Guizzetti, B. Andò, S. Baglio, C. Trigona, Improved energy harvesting from wideband vibrations by nonlinear piezoelectric converters, *Sensors and Actuators A: Physical* 162 (2) (2010) 425–431, doi:10.1016/j.sna.2010.05.022.
- [20] G. Litak, M. I. Friswell, S. Adhikari, Magnetopiezoelectric energy harvesting driven by random excitations, *Applied Physics Letters* 96 (21) 214103, doi:10.1063/1.3436553.
- [21] F. Qian, M. R. Hajj, L. Zuo, Bio-inspired bi-stable piezoelectric harvester for broadband vibration energy harvesting, *Energy Conversion and Management* 222 (2020) 113174, doi:10.1016/j.enconman.2020.113174.
- [22] A. Hajati, S.-G. Kim, Ultra-wide bandwidth piezoelectric energy harvesting, *Applied Physics Letters* 99 (8) (2011) 083105, doi:10.1063/1.3629551.
- [23] D. Mallick, A. Amann, S. Roy, A nonlinear stretching based electromagnetic energy harvester on FR4 for wideband operation, *Smart Materials and Structures* 24 (1) (2014) 015013, doi:10.1088/0964-1726/24/1/015013.
- [24] Y. Wu, A. Badel, F. Formosa, W. Liu, A. Agbossou, Nonlinear vibration energy harvesting device integrating mechanical stoppers used as synchronous mechanical switches, *Journal of Intelligent Material Systems and Structures* 25 (14) (2014) 1658–1663, doi:10.1177/1045389X14533437.
- [25] S. Kato, S. Ushiki, A. Masuda, A broadband energy harvester using leaf springs and stoppers with response stabilization control, *Journal of Physics: Conference Series* 1052 (2018) 012083, doi:10.1088/1742-6596/1052/1/012083.
- [26] F. Cottone, P. Basset, H. Vocca, L. Gammaitoni, Electromagnetic buckled beam oscillator for enhanced vibration energy harvesting, in: *2012 IEEE International Conference on Green Computing and Communications*, 624–627, doi:10.1109/GreenCom.2012.151, 2012.
- [27] R. Ramlan, M. J. Brennan, B. R. MacE, I. Kovacic, Potential benefits of a non-linear stiffness in an energy harvesting device, *Nonlinear Dynamics* 59 (4) (2010) 545–558, doi:10.1007/s11071-009-9561-5.
- [28] G. Sebald, H. Kuwano, D. Guyomar, B. Ducharne, Simulation of a Duffing oscillator for broadband piezoelectric energy harvesting, *Smart Materials and Structures* 20 (7), doi:10.1088/0964-1726/20/7/075022.
- [29] A. Cammarano, S. Neild, S. Burrow, D. Wagg, D. Inman, Optimum resistive loads for vibration-based electromagnetic energy harvesters with a stiffening nonlinearity, *Journal of Intelligent Material Systems and Structures* 25 (14) (2014) 1757–1770, doi:10.1177/1045389X14523854.

- [30] A. Cammarano, S. A. Neild, S. G. Burrow, D. J. Inman, The bandwidth of optimized nonlinear vibration-based energy harvesters, *Smart Materials and Structures* 23 (5) (2014) 055019, doi:10.1088/0964-1726/23/5/055019.
- [31] A. Masuda, A. Senda, A vibration energy harvester using a nonlinear oscillator with self-excitation capability, in: M. N. Ghasemi-Nejhad (Ed.), *Active and Passive Smart Structures and Integrated Systems 2011*, vol. 7977, International Society for Optics and Photonics, SPIE, 306–314, doi:10.1117/12.880905, 2011.
- [32] A. Masuda, A. Senda, T. Sanada, A. Sone, Global stabilization of high-energy response for a Duffing-type wideband nonlinear energy harvester via self-excitation and entrainment, *Journal of Intelligent Material Systems and Structures* 24 (13) (2013) 1598–1612, doi:10.1177/1045389X13479183.
- [33] A. Cammarano, A. Gonzalez-Buelga, S. A. Neild, S. G. Burrow, D. J. Inman, Bandwidth of a nonlinear harvester with optimized electrical load, *Journal of Physics: Conference Series* 476 (2013) 012071, doi:10.1088/1742-6596/476/1/012071.
- [34] S. Zhou, J. Cao, D. J. Inman, S. Liu, W. Wang, J. Lin, Impact-induced high-energy orbits of nonlinear energy harvesters, *Applied Physics Letters* 106 (9) (2015) 093901, doi:10.1063/1.4913606.
- [35] D. Mallick, A. Amann, S. Roy, Surfing the high energy output branch of nonlinear energy harvesters, *Phys. Rev. Lett.* 117 (2016) 197701, doi:10.1103/PhysRevLett.117.197701.
- [36] Lan, Chunbo, Tang, Lihua, Qin, Weiyang, Obtaining high-energy responses of nonlinear piezoelectric energy harvester by voltage impulse perturbations, *Eur. Phys. J. Appl. Phys.* 79 (2) (2017) 20902, doi:10.1051/epjap/2017170051.
- [37] A. Pasharavesh, M. T. Ahmadian, Toward Wideband Piezoelectric Harvesters Through Self-Powered Transitions to High-Energy Response, *Journal of Vibration and Acoustics* 142 (1), doi:10.1115/1.4045379.
- [38] Y. Zhang, C. Ding, J. Wang, J. Cao, High-energy orbit sliding mode control for nonlinear energy harvesting, *Nonlinear Dynamics* 105 (2021) 191–211, doi:10.1007/s11071-021-06616-8.
- [39] C. Saint-Martin, A. Morel, L. Charleux, E. Roux, A. Badel, Controlling orbits in nonlinear vibration energy harvesters dynamics, in: 10th European Nonlinear Dynamics Conference (ENOC) 2022, Lyon, France, 1–7, 2022.
- [40] N. Krylov, N. Bogoliubov, *Introduction to Non-linear Mechanics*, Princeton University Press, 1947.
- [41] H. K. Khalil, *Nonlinear Systems*, Macmillan Publishing, 1992.
- [42] Z. Yang, J. Zu, Z. Xu, Reversible nonlinear energy harvester tuned by tilting and enhanced by nonlinear circuits, *IEEE/ASME Transactions on Mechatronics* 21 (4) (2016) 2174–2184, doi:10.1109/TMECH.2016.2530619.
- [43] Z. Yang, Y. Zhu, J. Zu, Theoretical and experimental investigation of a nonlinear compressive-mode energy harvester with high power output under weak excitations, *Smart Materials and Structures* 24 (2) (2015) 025028, doi:10.1088/0964-1726/24/2/025028.
- [44] F. Cottone, P. Basset, H. Vocca, L. Gammaitoni, Electromagnetic buckled beam oscillator for enhanced vibration energy harvesting, *Proceedings - 2012 IEEE Int. Conf. on Green Computing and Communications, GreenCom 2012, Conf. on Internet of Things, iThings 2012 and Conf. on Cyber, Physical and Social Computing, CPSCom 2012* (2012) 624–627doi:10.1109/GreenCom.2012.151.
- [45] S. Roy, P. Podder, D. Mallick, Nonlinear energy harvesting using electromagnetic transduction for wide bandwidth, *IEEE Magnetics Letters* 7 (2016) 22–25, doi:10.1109/LMAG.2015.2509938.
- [46] P. Malatkar, A. Nayfeh, Calculation of the jump frequencies in the response of s.d.o.f. non-linear systems, *Journal of Sound and Vibration* 254 (5) (2002) 1005–1011, doi:10.1006/jsvi.2001.4104.
- [47] D. Zou, G. Liu, Z. Rao, T. Tan, W. Zhang, W.-H. Liao, A device capable of customizing nonlinear forces for vibration energy harvesting, vibration isolation, and nonlinear energy sink, *Mechanical Systems and Signal Processing* 147 (2021) 107101, doi:10.1016/j.ymsp.2020.107101.
- [48] D. Zou, G. Liu, Z. Rao, T. Tan, W. Zhang, W.-H. Liao, Design of vibration energy harvesters with customized nonlinear forces, *Mechanical Systems and Signal Processing* 153 (2021) 107526, doi:10.1016/j.ymsp.2020.107526.